

Laser opacity in underdense preplasma of solid targets due to quantum electrodynamics effects

W.-M. Wang,^{1,2} P. Gibbon,^{3,4} Z.-M. Sheng,^{5,6,7} Y.-T. Li,^{1,7,8} and J. Zhang^{6,7}

¹*Beijing National Laboratory for Condensed Matter Physics,
Institute of Physics, CAS, Beijing 100190, China*

²*Beijing Advanced Innovation Center for Imaging Technology,
Department of Physics, Capital Normal University, Beijing 100048, China*

³*Forschungszentrum Jülich GmbH, Institute for Advanced Simulation,
Jülich Supercomputing Centre, D-52425 Jülich, Germany*

⁴*Centre for Mathematical Plasma Astrophysics, Katholieke Universiteit Leuven, 3000 Leuven, Belgium*

⁵*SUPA, Department of Physics, University of Strathclyde, Glasgow G4 0NG, United Kingdom*

⁶*Key Laboratory for Laser Plasmas (MoE) and Department of Physics and Astronomy,
Shanghai Jiao Tong University, Shanghai 200240, China*

⁷*IFSA Collaborative Innovation Center, Shanghai Jiao Tong University, Shanghai 200240, China*

⁸*School of Physical Sciences, University of Chinese Academy of Sciences, Beijing 100190, China*

(Dated: December 17, 2019)

We investigate how next-generation laser pulses at 10 PW – 200 PW interact with a solid target in the presence of a relativistically underdense preplasma produced by amplified spontaneous emission (ASE). Laser hole boring and relativistic transparency are strongly restrained due to the generation of electron-positron pairs and γ -ray photons via quantum electrodynamics (QED) processes. A pair plasma with a density above the initial preplasma density is formed, counteracting the electron-free channel produced by the hole boring. This pair-dominated plasma can block the laser transport and trigger an avalanche-like QED cascade, efficiently transferring the laser energy to photons. This renders a 1- μm -scalelength, underdense preplasma completely opaque to laser pulses at this power level. The QED-induced opacity therefore sets much higher contrast requirements for such pulse in solid-target experiments than expected by classical plasma physics. Our simulations show for example, that proton acceleration from the rear of a solid with a preplasma would be strongly impaired.

Current developments in ultraintense pulsed laser technology indicate that laser pulses at the 100 PW level will be available in the near future. A number of laboratories worldwide are pursuing this high power frontier, such as the European Light Infrastructure (ELI), which is designed to deliver laser pulses of 100-200 PW [1], and the planned OMEGA EP-OPAL system which will supply 200 PW laser pulses [2]. Interaction of such ultra-relativistic pulses with matter will likely enter a QED-dominant regime. The plasma electrons can be instantly accelerated up to Lorentz factors $\gamma \sim a_0 > 1000$, where a_0 is the laser field strength normalized by $m_e c \omega_0 / e$ and ω_0 is the laser frequency. The QED parameter [3, 4] of $\chi_e \simeq \gamma F_{\perp} / (e E_S)$ will easily exceed 1, so that abundant γ -photons should be generated via Compton scattering, potentially offering an ultraintense γ -photon source [5, 6]. Here, $E_S = 1.32 \times 10^{18} \text{V/m}$ is the Schwinger field [7, 8] and F_{\perp} is the transverse component of the Lorentz force. The generated photons of high energy under the ultra-relativistic laser field, with the QED parameter of photons [3, 4] $\chi_{ph} \simeq (\hbar \omega / m_e c^2) F_{\perp} / (e E_S)$ approaching or exceeding 1, will strongly trigger a Breit-Wheeler process and create electron-positron pairs in an avalanche-like way [9–12], which can present the laser intensity upper limit attainable [10, 11] in the vacuum. This also provides a new approach for pair source generation [5, 13, 14].

On the other hand, when such a laser pulse is applied

in a solid target experiment, a preplasma produced by ASE could become more unavoidable [15, 16] than the case with a relatively low intensity pulse available currently. For example, as low as 10^{-11} ASE of a pulse at 10^{21}Wcm^{-2} can only produce a low level of preplasma ahead of a solid target [15, 16], which can be ignored in most cases. For a pulse at $10^{23} - 10^{25} \text{Wcm}^{-2}$, the same level of ASE (harder to achieve in technology) can produce a significant level of preplasma [15, 16]. Due to the preplasma production, it will be a challenge to make use of an extremely intense pulse in some key applications based on laser interaction with solid-density targets, such as ion acceleration via radiation pressure [17–22], high-order harmonic and attosecond pulse generation [23–25], or surface plasmon resonance [26–28], ect. Therefore, it is important to understand and anticipate the effects of a preplasma when a tightly focussed pulse at 10–200 PW irradiates a solid target, where the above-mentioned QED effects are expected to dominate.

In this Letter, we show that the QED effects can cause near complete energy depletion of such a pulse in a relativistically-underdense, small-scale preplasma. This contrasts to the regime studied to date where the preplasma is actually rendered *more* transparent because of laser hole boring and relativistic self-induced transparency [29]. At an early stage in the interaction, laser hole-boring acts within the leading edge of the pulse:

electrons are pushed away from the peak laser intensity zone by the ponderomotive force and an electron-free channel is formed in the preplasma. Under the combined charge-separation field and the ponderomotive force, oscillating electrons leave the peak intensity zone and cause abundant γ -photon generation, which cools the electrons and reduces the relativistic transparency. Later, a large number of pairs are created around the laser intensity peak zone, which fill the preplasma ion channel. The pair plasma can have a density much higher than the initial preplasma, which completely hinders further laser hole boring. This pair plasma strongly absorbs the laser energy and effectively transfers the energy to photons via the avalanche-like QED cascade [9–12]. In some case, the pair plasma density can be even higher than the relativistic critical density [29] and hence, the pulse is strongly reflected, which could enhance the QED cascade with the incident pulse together. The QED-induced inflation of the preplasma implies that significant improvements in laser contrast technology will be necessary before pulses with these intensities can be used in solid-target experiments. In particular, only a small fraction of the laser energy is finally absorbed by plasma electrons, which may significantly limit the conventional applications based on electrons pre-accelerated by laser pulses, e.g., ion acceleration.

Our investigation is carried out through particle-in-cell (PIC) simulations with the two-dimensional (2D) version of the KLAPS code [30, 31], in which γ -photon emission and pair creation via QED effects are included. A laser pulse is incident along the $+x$ direction with linear polarization along the y direction, wavelength $1 \mu\text{m}$ (or the period $\tau_0 = 2\pi/\omega_0 = 3.33 \text{ fs}$), spot radius $r_0 = 1 \mu\text{m}$, and duration 30 fs of full width at half maximum. Its peak power P_0 is 200 PW (P_0 from 10 PW to 180 PW will be also taken in the simulations below) and peak amplitude $a_0 = 3049$. A $0.5\text{-}\mu\text{m}$ -thick gold foil is taken, which is assumed to be composed of Au^{+10} ions and electrons with a density of $530 n_c$ ($n_c = 1.1 \times 10^{21} \text{ cm}^{-3}$) since we consider extremely intense pulses (a case with Au^{+15} ions and a higher electron density will be discussed below). In front of the foil there is a preplasma with an exponential density profile of a scalelength $L = 1 \mu\text{m}$ (L changing from $0.1 \mu\text{m}$ to $0.9 \mu\text{m}$ will also be taken below), which is expected to be produced by the laser ASE. The simulation box size $82\mu\text{m} \times 80\mu\text{m}$ in $x \times y$ directions is taken. Fourth-order algorithm for current calculation is employed [30, 32], with which the noise is well controlled. We take a spatial resolution of $0.0208 \mu\text{m}$ and 16 electrons and ions per cell. Because the particle number is not large initially, memory overflow is avoided in our simulations. The absorption budget of laser energy into the various kinds of particles is closely monitored during the simulation.

The red broken line in Fig. 1(a) is the simulation result without the QED effects. It shows that due to laser hole

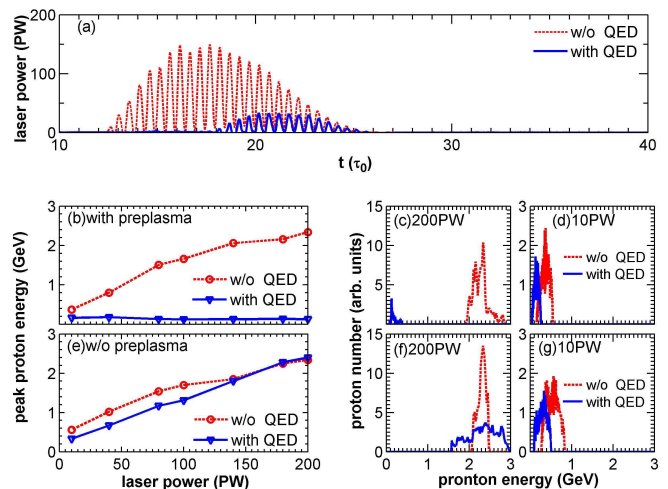


FIG. 1. (a) Temporal profile of the laser power passing through the preplasma rear. In (a)-(f) the red broken line and the blue solid line correspond to the simulations without and with the QED effects, respectively. [(b),(e)] Peak energy of the protons at $80 \tau_0$ versus the laser power. [(c),(d),(f),(g)] Proton energy spectra at $80 \tau_0$ with different laser powers. (b)-(d) are the results with a foil with a preplasma. (e)-(g) are the results with a polished foil without a preplasma.

boring and relativistic transparency, the 200 PW laser pulse with $a_0 = 3049$ easily penetrates through the preplasma with an average density $66n_c \ll a_0 n_c$ and a size of $8 \mu\text{m}$, retaining most of its initial energy. However, the pulse loses nearly all energy in the same preplasma if the QED effects are included, as seen in the blue line in Fig. 1(a). Only 8% initial laser energy (with 30 PW peak power) is transported through the preplasma; without the QED effects, the value is 65% (with 150 PW peak power).

The large difference of laser energy depletion in the preplasma results in quite different proton acceleration [see Figs. 1(b) and 1(c)], where a $0.05 \mu\text{m}$ thick proton layer of $50 n_c$ is located in the rear of the gold foil and the layer is $2 \mu\text{m}$ wide in the y -direction. The protons are accelerated to a peak energy of about 2.4 GeV at $80 \tau_0$ without the QED effects (note that we have not optimized target parameters for the proton acceleration). With the QED effects, the peak energy is reduced to 0.13 GeV because the depleted laser energy is mainly transferred to photons [see Fig. 2(a)], which do not contribute to the proton acceleration. As the laser power is decreased [see Figs. 1(d) and 1(b)], the difference of the proton energy is lessened between the two cases with and without the QED effects, since the QED-induced depletion is weakened. The protons are accelerated mainly via the target normal sheath acceleration (TNSA) [33] since nearly all energy of the pulse at 10-200 PW is depleted in the preplasma with the QED effects (as discussed below). Without the QED effects, TNSA and radiation

pressure acceleration work together since much laser energy is transported to the foil front.

In contrast to the results in Fig. 1(b) with the preplasma, Fig. 1(e) shows that the peak energy is continuously enhanced when a polished foil *without* the preplasma is taken. In this case, the peak energy shows little difference from the case without the QED effects. This is because when the foil is thin enough, the reaction of the foil to the pulse is weak and stays within a limited space, e.g., via the charge-separation field. In this case the foil electrons are mainly accelerated along the laser propagation direction, which is less effective in triggering Compton scattering for photon generation (see $\chi_e \simeq \gamma F_{\perp}/(eE_S)$ [3, 4]). Therefore, high energy protons/ions could be generated by 100-PW-class pulses, provided the laser contrast is sufficiently high and a thin enough foil is used. To optimize such proton/ion acceleration, one could match the foil thickness and the laser power as done in Ref. [34], but only after taking QED effects into account.

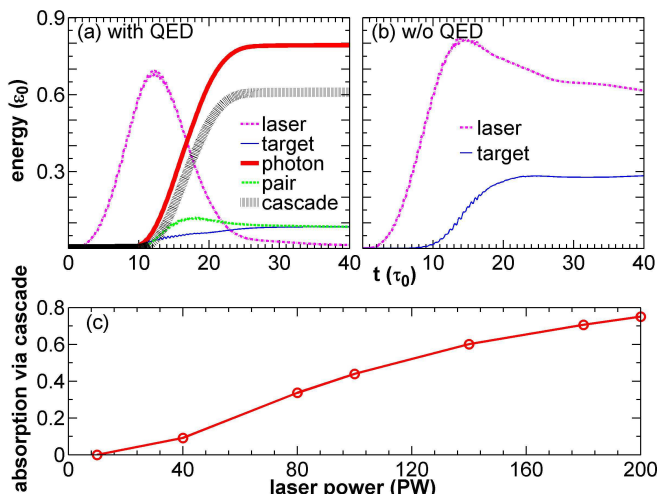


FIG. 2. [(a), (b)] Temporal evolution of residual energies of the laser pulse, target particles, photons, pairs, and the photons generated via the cascade (or only via the pairs), normalized by the total laser energy ε_0 , where the laser power is taken as 200 PW. Plots (a) and (b) correspond to the simulations with and without the QED effects, respectively. All particles escaped away from the simulation box are recorded and counted while the laser energy transported away is not counted. (c) Absorbed laser energy via the cascade in the preplasma region versus laser powers, where the energy is normalized by the total laser energy absorbed in this region.

In Fig. 2(a) the relative contributions of the generated photons and pairs, and the target particles (mainly the preplasma) to the laser energy depletion with the laser power of 200 PW are shown. About 80% laser energy is finally transferred to γ -photons. Firstly, some photons are generated around the laser axis at $y = 0$ [see Fig. 3(i)] via Compton scattering of the preplasma electrons after being accelerated by the pulse. The generated pho-

tons trigger the Breit-Wheeler process and create pairs in the peak laser intensity zone around the laser axis [see Fig. 3(i)]. Likewise, the pairs under the laser fields also generate Compton photons. In this way an avalanche-like cascade is formed causing copious photon generation. According to the black broken line in Fig. 2(a), 77% of the photons are generated via the pairs (or via the cascade) and the other 23% via the preplasma electrons. Therefore, the pairs or the cascade dominate the photon generation and the laser energy absorption over the preplasma electrons.

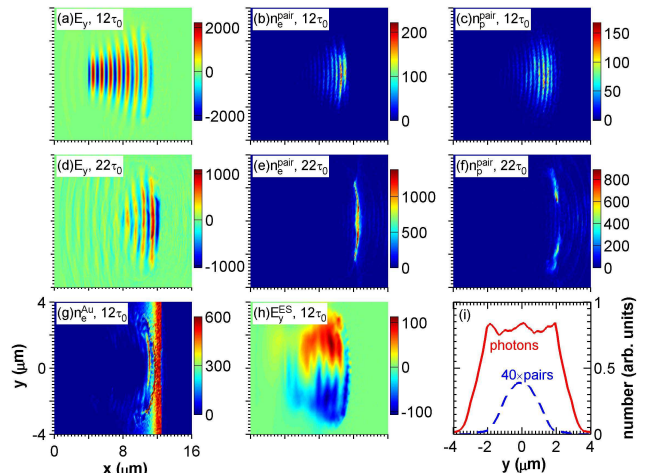


FIG. 3. Snapshots of laser electric fields $eE_y/m_e\omega_0c$ [(a), (d)], pair-plasma electron densities n_e^{pair}/n_c [(b), (e)] and positron densities n_p^{pair}/n_c [(c), (f)] at different times, Au-target electron density n_e^{Au}/n_c (g), and electrostatic field $eE_y^{ES}/m_e\omega_0c$ (h), where the maximum value is suppressed in (g) to show more clearly. (i) Number of the generated photons and pairs versus the transverse positions y , where the pair number is multiplied by a factor of 40.

There are two reasons for the cascade dominating the laser absorption. Firstly, the positrons, unlike massive ions, can be easily accelerated to ultra-relativistic energies and can thus contribute to the photon generation basically to the same extent as the electrons; they can also inhibit the acceleration of ions and protons. Secondly, due to requirement of the QED parameter $\chi_{ph} \simeq (\hbar\omega/m_e c^2)F_{\perp}/(eE_S)$ approaching or exceeding 1 [3, 4] for strong creation of pairs, most pairs are created in the peak laser intensity zone around the laser axis [see Figs. 3(i), 3(b) and 3(c)], basically where the photon generation rate is the highest. By contrast, the preplasma electrons are expelled away from this peak intensity zone [see Fig. 3(g)] via laser hole boring, within the pulse leading edge but mainly before the pair creation. This causes the reduction of photon generation via the preplasma electrons.

Due to the expelled electrons, a strong charge-separation field is formed around the laser axis [see Fig.

3(h)], which tends to keep the pair electrons within this region. Under this field, many freshly created pair electrons remain localized, leading to a growing pair-plasma electron density around the laser axis: it reaches about $1400 n_c$ at $22 \tau_0$, as seen in Figs. 3(e) and 3(b). Note that the charge-separation field also ensures that the positron densities are always lower than the pair-plasma electron densities, as seen in Figs. 3(c) and 3(f). In this way, the pair plasma fills the preplasma-electron-free channel and its density is much higher than the initial preplasma density, as seen in Figs. 3(g), 3(b), 3(c) and 3(e). Then, the laser hole boring and relativistic transparency can be completely inhibited. As the pulse strength a_0 is strongly reduced [see Fig. 3(d)], the density can be even higher than $a_0 n_c$ [see Fig. 3(e)], which causes the pulse to be significantly reflected. The reflected pulse with the incident one together can be quickly absorbed since they can strengthen the QED cascade [11, 12].

The contribution of the QED cascade to the laser depletion is weakened with decreasing laser power, as observed in Fig. 2(c). In this figure, we plot the laser absorption via the cascade (or only via the pairs). When the power is decreased to 100 PW from 200 PW, the contribution of the pairs to the laser absorption is reduced to 44% from 75%. The value is further reduced to about 10% at 40 PW. Therefore, in a $1\text{-}\mu\text{m}$ -scalelength preplasma, the cascade starts to be important at 40 PW and becomes the leading effect at around 100 PW.

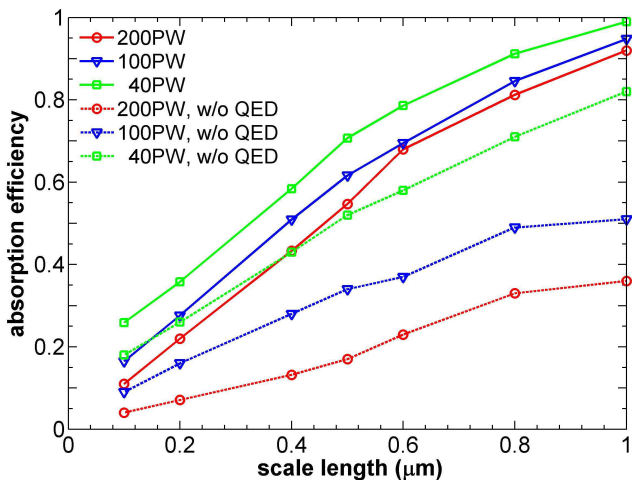


FIG. 4. The energy absorption efficiency of lasers with different powers in the preplasma region versus preplasma density scalelengths.

To gauge the sensitivity of this result to the initial preplasma density scalelength L and the laser power, a limited parameter scan of absorption efficiencies is depicted in Fig. 4, about which one can make several observations. First, one can see that QED effects generally result in much higher laser absorption for powers of 40–200 PW across the whole range of scalelengths considered

($L = 0.1\text{--}1.0\mu\text{m}$). Hence, much higher laser contrast will be required to apply such a pulse in future experiments than expected by classic plasma physics. The contrast between the two cases with and without the QED effects is reduced for lower powers, but the difference is still apparent even for relatively sharp profiles with $L = 0.1\mu\text{m}$. Second, with a smaller L (or a higher laser contrast) and a given power, less laser energy is depleted in the preplasma since the laser preplasma interaction zone is decreased. Third, with a lower power and a given L , the absorption efficiency of laser energy is higher. This is because the reaction of the preplasma to the lower-power pulse is comparatively stronger, i.e., a higher ratio of charge-separation field strength to the pulse strength and relatively more photons generated via the preplasma electrons, even though fewer photons are generated via the pairs or the cascade. To get 50% of the laser energy transported to the solid target front behind the preplasma according to Fig. 4, L should be around $0.5\mu\text{m}$ for the 200 PW pulse; and $L \simeq 0.4\mu\text{m}$ for the 100 PW and 40 PW pulses. When the Au^{+10} target is replaced by an Au^{+15} target, the laser depletion in the preplasma become stronger as seen in our simulations. This is because the Au^{+15} target and its preplasma with the same L have higher electron densities or more electrons.

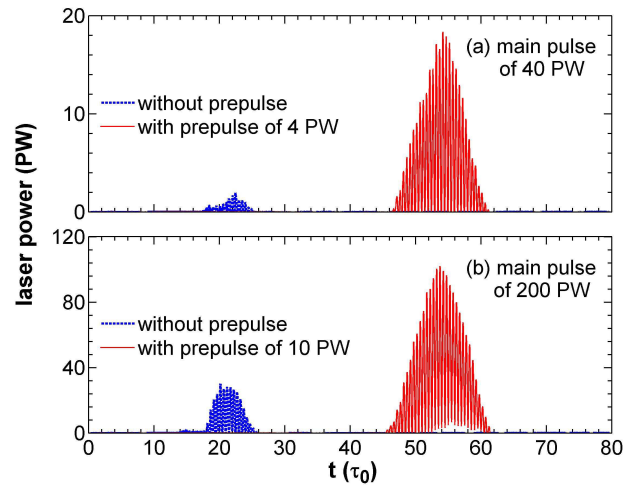


FIG. 5. Temporal profile of laser power passing through the preplasma rear, where a controlled prepulse is taken 120 fs ahead of the main pulse in the red line and no prepulse is taken in the blue broken line. (a) A 40 PW main pulse and a 4 PW prepulse are adopted. (b) A 200 PW main pulse and a 10 PW prepulse are adopted.

QED-induced preplasma inflation and the hinderance of the laser passage to the solid target surface can be mitigated by using a controlled prepulse. When the prepulse is ahead of the main one, it can create a nearly electron-free channel in the preplasma, reducing the interaction of the the main pulse with the preplasma electrons and consequently weakening the QED effects. In our simulations,

the prepulse and main pulse have the same duration 30 fs and spot radius $r_0 = 1 \mu\text{m}$ and an Au^{+10} target with a preplasma of $L = 1 \mu\text{m}$ is employed. In Fig. 5(a), when a 4 PW prepulse is taken, the 40 PW main pulse is transported through the preplasma with 18 times more energy (up to 36% initial energy of the main pulse) than the case without a prepulse. In Fig. 5(b), when a 10 PW prepulse is taken, the 200 PW main pulse is transported through the preplasma with 6 times more energy (up to 47% initial energy of the main pulse) than the case without a prepulse.

In summary, we have shown by PIC simulation that the QED effects can significantly enhance opacity of a laser pulse at 10-200 PW in a relativistically-transparent preplasma produced by ASE nearly unavoidable. A 1- μm -scalelength preplasma is completely opaque for such a pulse. To achieve transparencies above 50%, a preplasma with the scalelength below 0.4 μm is required. Therefore, the QED-induced opacity sets much higher demands on laser contrast technology for pulse powers of 10-200 PW than expected by classic plasma physics. We have illustrated that ahead of the main pulse, a controlled prepulse can effectively reduce such opacity, even if the prepulse power is far below the main pulse power.

The QED-induced opacity is most potent when a high-density pair plasma is formed around the peak laser intensity zone, to fill a preplasma-electron-free channel produced via laser hole boring. The pair plasma triggers an avalanche-like QED cascade to strongly absorb the laser energy, which finally transfers to photons. The cascade becomes the leading depletion mechanism and dominates over the depletion by preplasma electrons when the pulse power reaches 100 PW. It starts to be significant at 40 PW. Below 40 PW, the laser energy is depleted mainly due to pure Compton scattering via preplasma electrons. In any case, little laser energy is finally transferred to electrons of either the preplasma or the pairs, which shall significantly affect the applications based on electrons pre-accelerated by laser pulses, e.g., ion acceleration.

This work was supported by the National Basic Research Program of China (Grants No. 2013CBA01500) and NSFC (Grants No. 11375261, 11421064, 11374210, and 113111048). ZMS acknowledges the support of a Leverhulme Trust Research Grant and an EPSRC Grant No. EP/N028694/1).

[1] <http://www.extreme-light-infrastructure.eu>

[2] J. D. Zuegel, *Technology Development and Prospects for 100-PW-Class Optical Parametric Chirped-Pulse Amplification Pumped by OMEGA EP*, plenary talk at the 2nd International Symposium on High Power Laser Science and Engineering (HPLSE2016), March 15-18, 2016, Suzhou, China. (<http://www.hplse.net/dct/page/70005>)

- [3] T. Erber, *Rev. Mod. Phys.* **38**, 626 (1966).
- [4] N. V. Elkina, A. M. Fedotov, I. Yu. Kostyukov, M. V. Legkov, N. B. Narozhny, E. N. Nerush, and H. Ruhl, *Phys. Rev. ST Accel. Beams* **14**, 054401 (2011).
- [5] C. P. Ridgers, C. S. Brady, R. Ducloux, J. G. Kirk, K. Bennett, T. D. Arber, A. P. L. Robinson, and A. R. Bell, *Phys. Rev. Lett.* **108**, 165006 (2012).
- [6] C. S. Brady, C. P. Ridgers, T. D. Arber, A. R. Bell, and J. G. Kirk, *Phys. Rev. Lett.* **109**, 245006 (2012).
- [7] F. Sauter, *Z. Phys.* **69**, 742 (1931).
- [8] J. Schwinger, *Phys. Rev.* **82**, 664 (1951).
- [9] A. R. Bell and J. G. Kirk, *Phys. Rev. Lett.* **101**, 200403 (2008).
- [10] A. M. Fedotov, N. B. Narozhny, G. Mourou, and G. Korn, *Phys. Rev. Lett.* **105**, 080402 (2010).
- [11] S. S. Bulanov, T. Zh. Esirkepov, A. G. R. Thomas, J. K. Koga, and S. V. Bulanov, *Phys. Rev. Lett.* **105**, 220407 (2010).
- [12] E. N. Nerush, I. Y. Kostyukov, A. M. Fedotov, N. B. Narozhny, N. V. Elkina, and H. Ruhl, *Phys. Rev. Lett.* **106**, 035001 (2011).
- [13] I. V. Sokolov, N. M. Naumova, J. A. Nees, and G. A. Mourou, *Phys. Rev. Lett.* **105**, 195005 (2010).
- [14] M. Lobet, C. Ruyer, A. Debayle, E. d'Humieres, M. Grech, M. Lemoine, and L. Gremillet, *Phys. Rev. Lett.* **115**, 215003 (2015).
- [15] B. Dromey, S. Kar, M. Zepf and P. Foster, *Rev. Sci. Instrum.* **75**, 645 (2004).
- [16] O. Lundh, F. Lindau, A. Persson, and C.-G. Wahlstrom, P. McKenna, and D. Batani, *Phys. Rev. E* **76**, 026404 (2007).
- [17] T. Esirkepov, M. Borghesi, S. V. Bulanov, G. Mourou, and T. Tajima, *Phys. Rev. Lett.* **92**, 175003 (2004).
- [18] X. Q. Yan, C. Lin, Z. M. Sheng, Z. Y. Guo, B. C. Liu, Y. R. Lu, J. X. Fang, J. E. Chen, *Phys. Rev. Lett.* **100**, 135003 (2008).
- [19] A. P. L. Robinson, M. Zepf, S. Kar, R. G. Evans and C. Bellei, *New J. Phys.* **10**, 013021 (2008).
- [20] B. Shen, X. Zhang, Z.M. Sheng, M. Y. Yu, and J. Cary, *Phys. Rev. ST Accel. Beams* **12**, 121301 (2009).
- [21] L. L. Yu, H. Xu, W. M. Wang, Z. M. Sheng, B. F. Shen, W. Yu, and J. Zhang, *New J. Phys.* **12**, 045021 (2010).
- [22] F. L. Zheng, S. Z. Wu, H. C. Wu, C. T. Zhou, H. B. Cai, M. Y. Yu, T. Tajima, X. Q. Yan, and X. T. He, *Phys. Plasmas* **20**, 013107 (2013).
- [23] S. V. Bulanov, N. M. Naumova, and F. Pegoraro, *Phys. Plasmas* **1**, 745 (1994).
- [24] P. Gibbon, *Phys. Rev. Lett.* **76**, 50 (1996).
- [25] U. Teubner and P. Gibbon, *Rev. Mod. Phys.* **81**, 445 (2009).
- [26] S. Kahaly, S. Yadav, W.-M. Wang, S. Sengupta, Z. M. Sheng, A. Das, P. K. Kaw and G. R. Kumar, *Phys. Rev. Lett.* **101**, 145001 (2008).
- [27] W.-M. Wang, Z.-M. Sheng, and J. Zhang, *Phys. Plasmas* **15**, 030702 (2008).
- [28] S. Monchoce, S. Kahaly, A. Leblanc, L. Videau, P. Combis, F. Reau, D. Garzella, P. DOLiveira, Ph. Martin, and F. Quere, *Phys. Rev. Lett.* **112**, 145008 (2014).
- [29] P. Gibbon, *Short Pulse Laser Interactions with Matter* (Imperial College Press, London, 2000).
- [30] W.-M. Wang, P. Gibbon, Z.-M. Sheng, and Y.-T. Li, *Phys. Rev. E* **91**, 013101 (2015).
- [31] W.-M. Wang, Z.-M. Sheng, P. Gibbon, and Y.-T. Li, *Modeling of photon and pair generation due to quan-*

- tum electrodynamic effects in particle-in-cell simulation*
(<http://arxiv.org/abs/1608.06356>).
- [32] W.-M. Wang, P. Gibbon, Z.-M. Sheng, and Y.-T. Li, Phys. Rev. Lett. **114**, 015001 (2015).
- [33] M Borghesi, J Fuchs, S V Bulanov, A J Mackinnon, P K Patel, M Roth, Fusion Sci. Technol. **49**, 412 (2006).
- [34] T. Esirkepov, M. Yamagiwa, and T. Tajima, Phys. Rev. Lett. **96**, 105001 (2006).